

1 **Longitudinal double spin asymmetry of π^\pm -tagged jet,**
2 **Λ , $\bar{\Lambda}$, and K_S^0 in polarized $p + p$ collisions at $\sqrt{s} = 200$**
3 **GeV at STAR**

4 **Yi Yu, for the STAR Collaboration***

5 *^aInstitute of Frontier and Interdisciplinary Science & Key Laboratory of Particle Physics and Particle*
6 *Irradiation (Ministry of Education), Shandong University, Qingdao, Shandong 266237, China*

7 *E-mail: yuyikk@outlook.com*

8 Understanding the origin of the proton spin is one of the most fundamental and challenging questions in QCD. Much progress has been made since the first surprising result by the EMC experiment in the late 1980s. However, the helicity distributions of strange quarks and anti-quarks inside the proton are still not well constrained by the experimental data. Measurement of the longitudinal double spin asymmetry A_{LL} of the inclusive jets tagged with a π^\pm/π^- carrying high jet momentum fraction, z , in $p + p$ collisions can provide further constraints on the gluon helicity distribution in the proton. In addition, the A_{LL} of Λ , $\bar{\Lambda}$ and K_S^0 in the longitudinally polarized $p + p$ collisions may shed light on the strange quark and anti-quark helicity distributions. In this contribution, we report the preliminary results on the A_{LL} measurements of inclusive jets tagged with a high- z π^\pm , and the Λ , $\bar{\Lambda}$ and K_S^0 . We utilize the longitudinally polarized $p + p$ collisions at $\sqrt{s} = 200$ GeV collected by the STAR experiment with an integrated luminosity of about 52 pb^{-1} .

25th International Spin Physics Symposium (SPIN 2023)
24-29 September 2023
Durham, NC, USA

*Speaker

9 1. Introduction

10 Inspired by the first surprising results of the proton spin structure from the EMC Collabo-
 11 ration [1], tremendous progress has been made in the past 35 years to improve our knowledge of
 12 how the proton spin is made up by the quarks and gluons in Quantum Chromodynamics (QCD).
 13 Nevertheless, there still remain open questions that challenge the current understanding of the com-
 14 position of the proton spin. In polarized $p + p$ collisions, the longitudinal double spin asymmetry
 15 A_{LL} is expected to be sensitive to the helicity distributions of partons inside the proton, which is
 16 defined as the difference between the cross section with same and opposite beam helicity:

$$A_{LL} \equiv \frac{\sigma^{++} - \sigma^{+-}}{\sigma^{++} + \sigma^{+-}} = \frac{\Delta\sigma}{\sigma} \quad (1)$$

17 At leading order, the $\Delta\sigma$ is proportional to $\Delta f_1 \Delta f_2 \hat{a}_{LL}$, where Δf_1 and Δf_2 are the helicity
 18 distributions of two colliding partons and \hat{a}_{LL} is the double spin asymmetry at partonic level and
 19 can be calculated by the perturbative QCD.

20 The Relativistic Heavy Ion Collider (RHIC) is the world's first and only polarized $p + p$
 21 collider and is capable of colliding both longitudinally and transversely polarized proton beams
 22 at $\sqrt{s} = 200$ GeV and 500 GeV. The dominant subprocesses of the hard scattering in such $p + p$
 23 collisions are quark-gluon and gluon-gluon scatterings [2], which make RHIC an ideal facility to
 24 study the gluon helicity distribution. Series of A_{LL} measurements [2–7] for jets and dijets have
 25 confirmed a sizable gluon polarization [8, 9] inside the longitudinally polarized proton. However,
 26 the JAM Collaboration recently proposed that A_{LL} of inclusive jets is not sensitive to the sign
 27 of the gluon helicity distribution and a negative gluon polarization is also allowed [10]. As the
 28 helicity distributions of u quark and d quark are in opposite sign, and they favor π^+ and π^- in the
 29 hadronization, respectively, A_{LL} of the π^\pm -tagged jets is expected to be sensitive to the sign of the
 30 gluon helicity. In addition, the helicity distributions of the strange quark and anti-quark [9, 11] are
 31 still poorly constrained by the experiments. Measuring the longitudinal double spin asymmetry of
 32 Λ hyperons and K_S^0 can shed light on the strange quark and anti-quark helicity distributions.

33 In 2015, STAR concluded its longitudinal polarized data collection at $\sqrt{s} = 200$ GeV. This data
 34 set corresponds to an integrated luminosity of about 52 pb^{-1} with an average beam polarization of
 35 about 54%. With this data set, we performed the first measurement of the A_{LL} for the π^\pm -tagged
 36 jet, Λ hyperons, and K_S^0 .

37 2. Longitudinal Double Spin Asymmetry A_{LL} of π^\pm -tagged Jet

38 2.1 Jet Reconstruction

39 Similar to previous publications from STAR [2, 5, 6], jets were reconstructed with charged-
 40 particle tracks measured by the Time Projection Chamber (TPC) [12] and the energy deposits in
 41 the Barrel Electromagnetic Calorimeter (BEMC) [13] and the Endcap Electromagnetic Calorimeter
 42 (EEMC) [14] using the anti- k_T algorithm [15] with a resolution parameter $R = 0.6$. An off-axis cone
 43 method adapted from the ALICE experiment [16] was used to correct the transverse momentum p_T
 44 of the reconstructed jet for the contribution of the underlying events. A Monte Carlo simulation
 45 sample was generated to correct the reconstructed jet quantities back to particle level and estimate

46 systematic uncertainties in these measurements. In the simulation, the $p + p$ collision events
 47 were generated with PYTHIA6 [17] and were further processed through a STAR detector-response
 48 package based on GEANT3 [18]. The simulated events were then embedded into the zero-bias
 49 events recorded during the STAR data-taking runs to simulate the pile-ups and beam backgrounds
 50 present in data. Same jet reconstruction procedure was applied to this simulation sample. In
 51 addition, particle-level jets were reconstructed and the jet p_T in data was corrected back to particle
 52 level.

53 2.2 π^\pm Identification

54 In this measurement, charged pions were identified based on their energy loss dE/dx inside
 55 the TPC. At STAR, the dE/dx is normalized into $n\sigma$ according to the following formula:

$$n\sigma(\pi) = \frac{1}{\sigma_{\text{exp}}} \ln \left(\frac{dE/dx_{\text{obs}}}{dE/dx_{\pi, \text{cal}}} \right), \quad (2)$$

56 where the dE/dx_{obs} and the $dE/dx_{\pi, \text{cal}}$ are the measured energy loss of the tracks and the expected
 57 energy loss of the π^\pm based on the Bichsel formalism [19]. The σ_{exp} is the energy loss resolution of
 the TPC [20, 21]. In practice, the $n\sigma(\pi)$ distribution was divided into three particle-rich regions, i.e.,

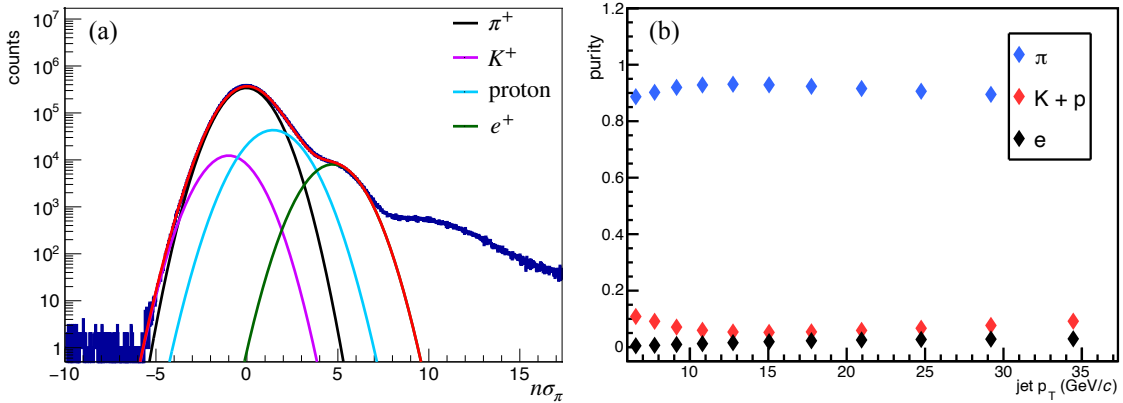


Figure 1: (a) Multi-Gaussian fitting on the $n\sigma(\pi)$ distribution for positive charged tracks with their momentum $1.4 < p < 1.5$ GeV/c. (b) Particle purity as a function of jet transverse momentum p_T in pion-rich region for positive charged tracks carrying jet momentum fraction $z > 0.2$.

58 pion-rich region, kaon+proton-rich region, and electron-rich region. Similar to [22], particle purity
 59 at each particle-rich region was estimated with a multi-Gaussian fitting to the $n\sigma(\pi)$ distribution of
 60 charged tracks. Figure 1(a) shows an example of the multi-Gaussian fitting of the $n\sigma(\pi)$ distribution
 61 for positive charged tracks with their momentum $1.4 < p < 1.5$ GeV/c. The estimated purity, for
 62 example, as a function of jet p_T in pion-rich region is presented in Fig. 1(b). To enhance the fraction
 63 of jets from the fragmentation of u quark and d quark, jet momentum fraction $z \equiv \vec{p}_\pi \cdot \vec{p}_{jet} / |\vec{p}_{jet}|^2$
 64 carried by the π^\pm was required to be larger than 0.2.
 65

66 2.3 A_{LL} Extraction & Result

67 Experimentally, the longitudinal double asymmetry A_{LL} can be calculated with the following
 68 formula:

$$A_{LL} = \frac{1}{P_Y P_B} \frac{N^{++} - \mathcal{R} N^{+-}}{N^{++} + \mathcal{R} N^{+-}}, \quad (3)$$

69 where P_Y and P_B are the measured polarization of two colliding beams. N^{++} and N^{+-} are the
 70 π^\pm -tagged jet yields from beam bunches with same and opposite beam helicity configurations,
 71 respectively. \mathcal{R} is the relative luminosity measured by the Vertex Position Detectors (VPD) [23] and
 72 the Zero Degree Calorimeters (ZDC) [24]. The raw asymmetry, A_{LL}^{raw} , calculated from each particle
 73 rich region is expected to be a linear combination of the A_{LL} of each particles. The π^\pm -tagged A_{LL}
 74 can be obtained by solving the following linear equations:

$$\begin{bmatrix} f_{\pi_{\text{rich}}}^\pi & f_{\pi_{\text{rich}}}^{K+p} & f_{\pi_{\text{rich}}}^e \\ f_{K+p_{\text{rich}}}^\pi & f_{K+p_{\text{rich}}}^{K+p} & f_{K+p_{\text{rich}}}^e \\ f_{e_{\text{rich}}}^\pi & f_{e_{\text{rich}}}^{K+p} & f_{e_{\text{rich}}}^e \end{bmatrix} \begin{bmatrix} A_{LL}^\pi \\ A_{LL}^{K+p} \\ A_{LL}^e \end{bmatrix} = \begin{bmatrix} A_{LL}^{\text{raw}, \pi_{\text{rich}}} \\ A_{LL}^{\text{raw}, K+p_{\text{rich}}} \\ A_{LL}^{\text{raw}, e_{\text{rich}}} \end{bmatrix}, \quad (4)$$

75 where, for example, $f_{\pi_{\text{rich}}}^\pi$ is the π^\pm purity at π^\pm rich region.

76 The preliminary results of the π^\pm -tagged jet A_{LL} with jet momentum fraction $z > 0.2$ and
 77 $z > 0.3$ are presented in Fig. 2 (a) and Fig. 2 (b), respectively. Predictions based on PYTHIA6 [17]
 78 and the helicity distributions from NNPDF Collaboration [9] are compared with the measurements.
 79 The measurements are consistent with the predictions of $A_{LL}^{\pi^+} > A_{LL}^{\pi^-}$ with positive gluon helicity.

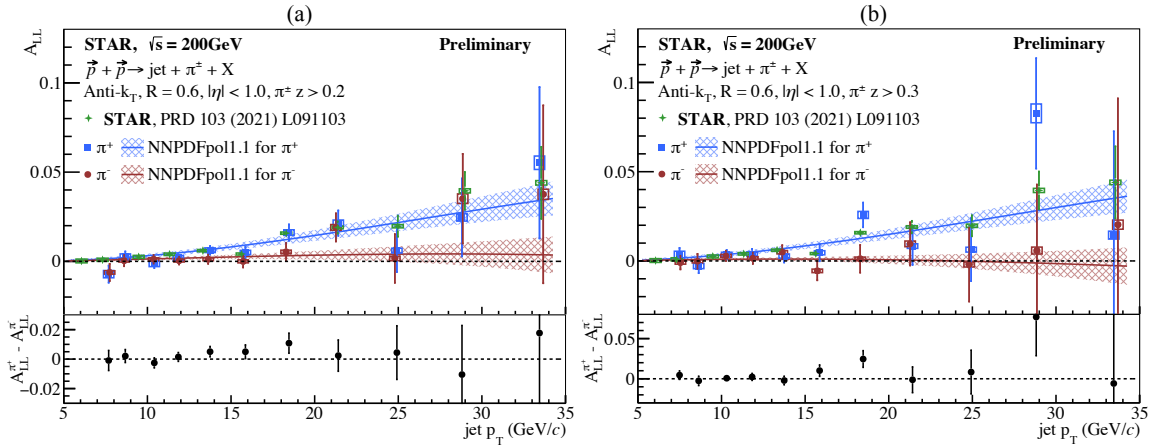


Figure 2: Panel (a) and (b): preliminary results of the longitudinal double spin asymmetry A_{LL} of the π^\pm -tagged jet as a function of jet p_T in polarized $p + p$ collisions at $\sqrt{s} = 200$ GeV with jet momentum fraction $z > 0.2$ and $z > 0.3$, respectively. The bars represent the statistical uncertainties while the systematic uncertainties are shown in boxes. Predictions calculated with the helicity distributions [9] based on PYTHIA6 [17] are compared to data.

80 3. Longitudinal Double Spin Asymmetry of Λ , $\bar{\Lambda}$ and K_S^0

81 3.1 Λ , $\bar{\Lambda}$ and K_S^0 Reconstruction

82 The Λ ($\bar{\Lambda}$) hyperons and K_S^0 were reconstructed via their decay channels $\Lambda \rightarrow p + \pi^-$ ($\bar{\Lambda} \rightarrow$
 83 $\bar{p} + \pi^+$), and $K_S^0 \rightarrow \pi^+ + \pi^-$, respectively. Daughter tracks were identified based on their energy
 84 loss dE/dx inside the TPC. Two daughter candidates were paired firstly and a set of selection
 85 criteria was applied based on the decay topology of the Λ hyperons and K_S^0 . Figure 3 shows the
 86 invariant mass distribution of the reconstructed Λ , $\bar{\Lambda}$, and K_S^0 candidates at $3 < p_T < 4$ GeV/ c .
 87 The residual backgrounds under their mass peak are mainly from the random combination of two
 88 daughter candidates and were estimated with the side-band method.

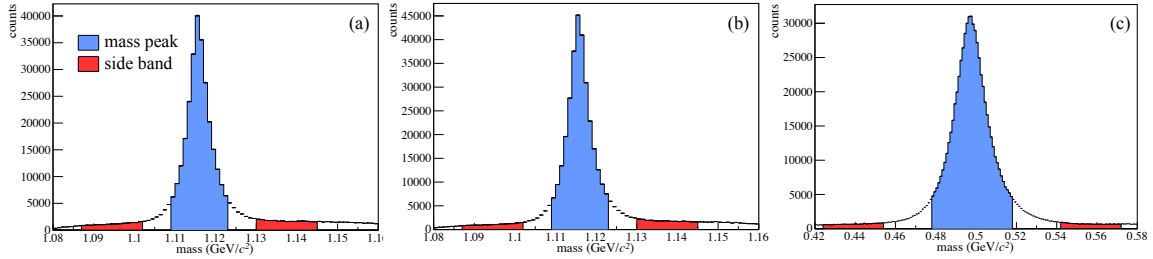


Figure 3: Panel (a), (b) and (c) show the invariant mass distributions of the reconstructed Λ , $\bar{\Lambda}$ and K_S^0 candidates at $3 < p_T < 4$ GeV/ c , respectively. The yields under the mass peak (blue-filled area) are used for the A_{LL}^{raw} calculation and the yields under the side-band region (red-filled area) are used for estimating the background fraction under the mass peak.

89 The reconstructed Λ , $\bar{\Lambda}$ and K_S^0 candidates were used as inputs in the jet reconstruction using
 90 the same method as in Ref. [25]. In-jet Λ hyperons and K_S^0 were used for further analysis to make
 91 sure Λ hyperons and K_S^0 originate from a hard partonic scattering.

92 3.2 A_{LL} Extraction & Result

93 Similarly, the longitudinal double spin asymmetry of the Λ hyperons and the K_S^0 can be
 94 measured with the Eq. (3). The A_{LL}^{raw} from mass peak and the A_{LL}^{bkg} from the side-band region were
 95 extracted separately with the Eq. (3). The influence of the residual backgrounds was corrected with
 96 the following formula:

$$A_{LL} = \frac{A_{LL}^{raw} - r A_{LL}^{bkg}}{1 - r}, \quad (5)$$

97 where r is the residual background fraction under mass peak and is found to be below 10%.

98 The preliminary results of the longitudinal double spin asymmetry of the in-jet Λ hyperons
 99 and K_S^0 as a function of particle p_T are presented in Fig. 4. The results are consistent with zero
 100 within uncertainties. Figure 5 shows the A_{LL} as a function of the jet p_T . The jet momentum
 101 fraction z shown on the bottom panel was corrected back to particle level with the same Monte
 102 Carlo simulation samples used in π^\pm -tagged jet A_{LL} measurements. The jet sample used in Fig. 5
 103 has large overlap with the published inclusive jet A_{LL} measurement [5], but this result is more
 104 sensitive to the strange quark and anti-quark helicity distributions as Λ hyperons and K_S^0 are a part

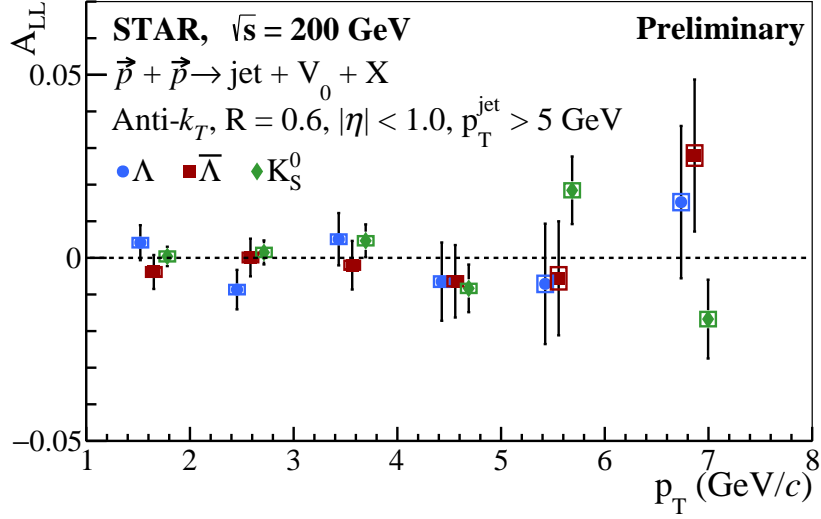


Figure 4: Preliminary results of longitudinal double spin asymmetry A_{LL} as a function of particle p_T for Λ , $\bar{\Lambda}$, and K_S^0 in polarized $p + p$ collisions at $\sqrt{s} = 200$ GeV. The results of $\bar{\Lambda}$ and K_S^0 have been slightly offset horizontally for clarity.

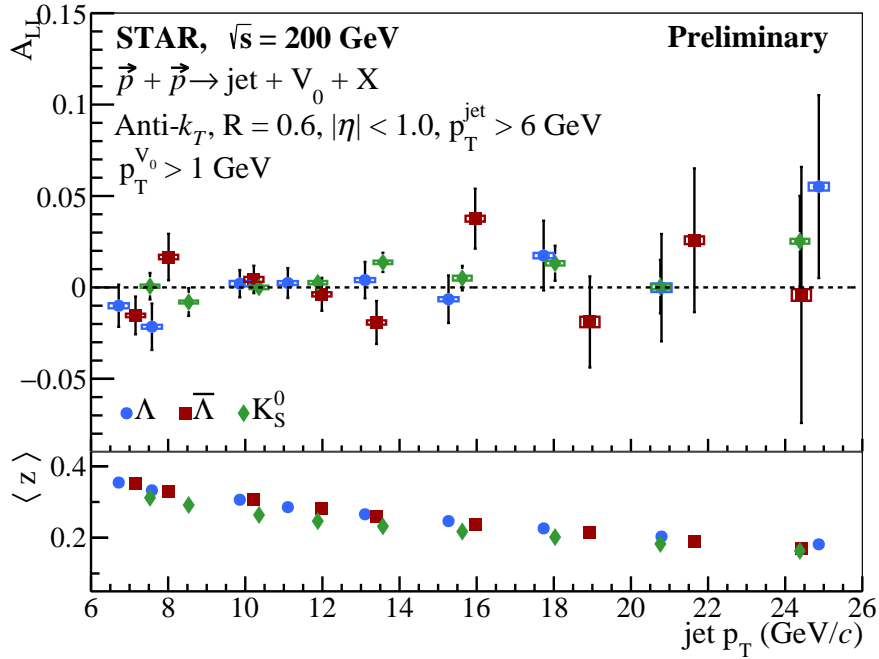


Figure 5: Top panel: preliminary results of longitudinal double spin asymmetry A_{LL} as a function of jet p_T for Λ , $\bar{\Lambda}$, and K_S^0 in polarized $p + p$ collisions at $\sqrt{s} = 200$ GeV. Bottom panel: the averaged particle-level jet momentum fraction z carried by Λ hyperons and K_S^0 .

105 of jet. Another related analysis is the longitudinal spin transfer of the Λ hyperons, which is also
106 sensitive to the strange quark and anti-quark helicity distributions [25]. Small A_{LL} results might
107 indicate small strange quark and anti-quark helicity distributions inside the proton.

108 4. Summary

109 We reported new preliminary results of the longitudinal double spin asymmetry A_{LL} of the
110 π^\pm -tagged jet, Λ hyperons, and K_S^0 in polarized $p + p$ collisions at $\sqrt{s} = 200$ GeV at STAR. The
111 π^\pm -tagged jet A_{LL} can provide sensitivity to the sign of the gluon helicity distribution. The results
112 indicate $A_{LL}^{\pi^+} > A_{LL}^{\pi^-}$, which favor positive gluon helicity. The first measurement of A_{LL} for the
113 in-jet Λ hyperons and K_S^0 is consistent with zero within uncertainties, which indicates small helicity
114 distribution of the strange quark and anti-quark inside the proton.

115 Acknowledgements

116 The author is supported partially by the National Natural Science Foundation of China under
117 No. 12075140.

118 References

- 119 [1] J. Ashman et al. *Phys. Lett. B*, **206**(2):364–370, 1988.
- 120 [2] J. Adam et al. [STAR Collaboration]. *Phys. Rev. D*, **100**(5):052005, 2019.
- 121 [3] L. Adamczyk et al. [STAR Collaboration]. *Phys. Rev. Lett.*, **115**(9):092002, 2015.
- 122 [4] J. Adam et al. [STAR Collaboration]. *Phys. Rev. D*, **98**(3):032011, 2018.
- 123 [5] M. S. Abdallah et al. [STAR Collaboration]. *Phys. Rev. D*, **103**(9):L091103, 2021.
- 124 [6] M. S. Abdallah et al. [STAR Collaboration]. *Phys. Rev. D*, **105**(9):092011, 2022.
- 125 [7] Z. Chang and T. Lin. *arXiv*, 2306.11306, 2023.
- 126 [8] D. de Florian, R. Sassot, M. Stratmann, and W. Vogelsang. *Phys. Rev. Lett.*, **113**(1):012001,
127 2014.
- 128 [9] E. R. Nocera et al. *Nucl. Phys. B*, **887**:276–308, 2014.
- 129 [10] Y. Zhou, N. Sato, and W. Melnitchouk. [JAM Collaboration]. *Phys. Rev. D*, **105**(7):074022,
130 2022.
- 131 [11] J. J. Ethier, N. Sato, and W. Melnitchouk. [JAM Collaboration]. *Phys. Rev. Lett.*,
132 **119**(13):132001, 2017.
- 133 [12] M. Anderson et al. *Nucl. Instrum. Methods Phys. Res., Sect. A*, **499**(2-3):659–678, 2003.
- 134 [13] M. Beddo et al. *Nucl. Instrum. Methods Phys. Res., Sect. A*, **499**(2-3):725–739, 2003.

- 135 [14] C. E. Allgower et al. *Nucl. Instrum. Methods Phys. Res., Sect. A*, **499**(2-3):740–750, 2003.
- 136 [15] M. Cacciari, G. P. Salam, and G. Soyez. *J. High Energy Phys.*, **2008**(04):063–063, 2008.
- 137 [16] B. Abelev et al. [ALICE Collaboration]. *Phys. Rev. D*, **91**(11):112012, 2015.
- 138 [17] T. Sjöstrand, S. Mrenna, and P. Skands. *J. High Energy Phys.*, **2006**(05):026, 2006.
- 139 [18] R. Brun et al. CERN, rev. version edition, 1987.
- 140 [19] Hans Bichsel. *Nucl. Instrum. Methods Phys. Res., Sect. A*, **562**(1):154–197, 2006.
- 141 [20] Yichun Xu et al. *Nucl. Instrum. Methods Phys. Res., Sect. A*, **614**(1):28–33, 2010.
- 142 [21] Ming Shao et al. *Nucl. Instrum. Methods Phys. Res., Sect. A*, **558**(2):419–429, 2006.
- 143 [22] M. S. Abdallah et al. [STAR Collaboration]. *Phys. Rev. D*, **106**(7):072010, 2022.
- 144 [23] W. J. Llope. *Nucl. Instrum. Methods Phys. Res., Sect. A*, **759**:23, 2014.
- 145 [24] C. Adler et al. *Nucl. Instrum. Methods Phys. Res., Sect. A*, **470**:488, 2001.
- 146 [25] M. I. Abdulhamid et al. [STAR Collaboration]. *Phys. Rev. D*, **109**(1):012004, 2024.